



Advances in Reduced order modelling for CFD: vortex shedding around a circular cylinder using a POD-Galerkin method

Giovanni Stabile^{1*}, Saddam Hijazi¹, Andrea Mola¹, Stefano Lorenzi²,
Gianluigi Rozza¹

¹SISSA, International School for Advanced Studies, Mathematics Area, mathLab
Trieste, Italy

²Department of Energy, Politecnico di Milano, Italy

*Email address for correspondence: gstable@sissa.it

Communicated by Associate Editor

Received on 10 01, 2017. Accepted on XXXX XX, XXXX.

Abstract

Vortex shedding around circular cylinders is a well known and studied phenomenon that appears in many engineering fields. In this work a Reduced Order Model (ROM) of the incompressible flow around a circular cylinder, built performing a Galerkin projection of the governing equations onto a lower dimensional space is presented. The reduced basis space is generated using a Proper Orthogonal Decomposition (POD) approach. In particular the focus is into (i) the correct reproduction of the pressure field, that in case of the vortex shedding phenomenon, is of primary importance for the calculation of the drag and lift coefficients; (ii) for this purpose the projection of the Governing equations (momentum equation and Poisson equation for pressure) is performed onto different reduced basis space for velocity and pressure, respectively; (iii) all the relevant modifications necessary to adapt standard finite element POD-Galerkin methods to a finite volume framework are presented. The accuracy of the reduced order model is assessed against full order results.

Keywords: ROM, POD-Galerkin, Finite Volumes, CFD, vortex shedding

AMS subject classification: 78M34, 97N40, 35Q35

1. Introduction

A large part of physical systems is described by partial differential equations and their numerical solution is essential in many engineering fields. Even though in the last decades several progresses have been done in the numerical analysis community, in the case of fluid dynamics problems, the numerical solution of the governing equations, using standard finite element

methods (FEM), spectral element methods (SEM), finite volume methods (FVM) or finite differences methods (FDM), may be computationally extremely expensive. The development of efficient and reliable Reduced Order Models (ROMs) could be a great advantage especially dealing with control, optimization and uncertainty quantification problems, where a large number of different system configurations are in need of being tested.

Vortex Induced Vibrations (VIVs) are important phenomena in many different engineering fields like bridges, offshore environments, transmission lines and marine cables and have been studied in either air or water for many years [1,2]. The importance of studying such a problem comes from the fact that it can be the source of evident damage or failure of the engineering system. Not to consider VIVs through the design process can lead to severe effects. This phenomenon is caused by the oscillating flow arising from the alternate vortex shedding. Among all possible existing phenomena that may happen on flexible cylindrical structures, VIVs are one of the most dangerous and hard to predict. If a rigid and fixed cylinder is considered, the frequency of the vortex shedding phenomenon follows the *Strouhal* law $St = f_v D / U$ [3] in which St is the *Strouhal* number, f_v is the frequency of the vortex shedding, U is the free stream velocity and D is the diameter of the cylinder.

For a rigid and fixed circular cylinder the *Strouhal* number, over a certain range of the *Reynolds* number, assumes a constant value approximately equal to 0.2. In this range of values ($10^2 \lesssim Re \lesssim 10^5$), which are particularly interesting for practical applications, the relationship between the free stream velocity and frequency of vortex shedding is linear. Conversely, if a cylinder, which is free to vibrate or forced to move, is considered, the phenomenon cannot be well represented by the *Strouhal* law. When the vortex shedding frequency approaches the natural frequency, the so called lock-in phenomenon is observed. The synchronisation of the vortex shedding frequency to the frequency of oscillation occurs over a certain range of the flow velocity. In this range the vortex shedding phenomenon is driven by the frequency of oscillation of the cylinder.

For the particular case of the vortex shedding phenomenon around a circular cylinder one can find several attempts to create a ROM. In some cases no attempt to model completely the flow field is done such as in [4–6] where only the lift and drag forces acting on the cylinder are modelled using wake oscillator models. When the interest is into the complete reconstruction of the flow field, Reduced Basis (RB) method can be applied. In this method the governing equations, describing the phenomenon, are projected onto a low dimensional space called the reduced basis space [7,8] that is optimally constructed starting from high fidelity simulations. In particular in

this work the ROM is constructed using a POD-Galerkin approach [9–11].

The work is organized as follows. In § 2 the governing equations of the physical model and the high fidelity (HF) discretisation techniques used to solve the full order model are presented. The development of the ROM is introduced in § 3 and in § 4 the numerical example, regarding the vortex shedding phenomenon around a circular cylinder, is analysed. Finally in § 5 conclusions and suggestions for future developments are given.

2. The Full Order Model

The physical model is described below by using the incompressible unsteady Navier-Stokes equations. They consists into the well known conservation of momentum law and continuity equations. In an Eulerian framework they are expressed by:

$$(1) \quad \begin{cases} \frac{\partial \mathbf{u}}{\partial t} + (\mathbf{u} \cdot \nabla) \mathbf{u} - \nabla \cdot \nu \nabla \mathbf{u} = -\nabla p & \text{in } \Omega_f \times [0, T] \\ \nabla \cdot \mathbf{u} = 0 & \text{in } \Omega_f \times [0, T], \end{cases}$$

in which \mathbf{u} is the flow velocity vector, t is the time, ν is the fluid kinematic viscosity, and p is the normalized pressure, which is divided by the fluid density ρ_f , Ω_f is the fluid domain, and T is the time window we considered. In the present work the problem is solved using using a finite volume discretisation technique [12,13]. This discretization technique became the standard for industrial applications with increasing *Reynolds* numbers and permits local enforcement of the conservative law since equations are written in conservative form. In particular in this work the finite volume C++ library OpenFOAM[®] (OF) [14] is used.

2.1. The Finite Volume discretisation

As mentioned in § 1 the governing equations are discretised in space using a finite volume approximation. Once a suitable tessellation is chosen, the system of partial differential equations in (1) are written in integral form over a control volume. The dimension of the full order model, which consists into the number of degrees of freedom of the discretized problem, will be henceforth indicated with N_h . The strategies for the discretisation of both the momentum and continuity equation are briefly recalled in the following.

2.1.1. Momentum equation

The momentum equation is rewritten for each volume V_i in integral form as:

$$(2) \quad \int_{V_i} \frac{\partial}{\partial t} \mathbf{u} dV + \int_{V_i} (\mathbf{u} \cdot \nabla) \mathbf{u} dV - \int_{V_i} \nabla \cdot \nu \nabla \mathbf{u} dV + \int_{V_i} \nabla p dV = 0.$$

The convective term making use of the Gauss's theorem is discretised as follow:

$$(3) \quad \int_{V_i} (\mathbf{u} \cdot \nabla) \mathbf{u} dV = \int_{S_i} d\mathbf{S} \cdot \mathbf{u}_f \mathbf{u}_f \approx \sum_f \mathbf{S}_f \cdot \mathbf{u}_f \mathbf{u}_f = \sum_f F_f u_f,$$

where \mathbf{S}_f is the area vector of each face of the control volume (Figure 1), \mathbf{u}_f is the velocity vector evaluated at the center of each face of the control volume, and F_f is the mass flux trough each face of the control volume. The diffusion term is then discretised as:

$$(4) \quad \int_{V_i} \nabla \cdot \nu \nabla \mathbf{u} dV = \int_{S_i} d\mathbf{S} \cdot \nu \nabla \mathbf{u} \approx \sum_f \nu \mathbf{S}_f \cdot (\nabla \mathbf{u})_f,$$

where the gradient at the face $(\nabla \mathbf{u})_f$ is evaluated using an implicit scheme with the addition of an explicit term to account for the non-orthogonality between the vector connecting the centre of two neighbouring cells and the face dividing them. For further details one may see the OF documentation [15]. The gradient of pressure is discretised as:

$$(5) \quad \int_{V_i} \nabla p dV = \int_{S_i} d\mathbf{S} \cdot \mathbf{p} \approx \sum_f \mathbf{S}_f p_f.$$

2.1.2. Continuity equation

The coupling between momentum conservation and continuity equation is treated making use of a segregated approach. The PIMPLE algorithm [13] is used, it consists into a combination of an inner correction cycle using the PISO [16] algorithm and an outer correction procedure performed using the SIMPLE [17] algorithm. The two considered equations are the momentum equation and the Poisson equation for pressure, which is obtained taking the divergence of the momentum equation and exploiting the continuity equation:

$$(6) \quad \Delta p = -\nabla \cdot (\mathbf{u} \cdot \nabla) \mathbf{u}.$$

The same approach is used also at reduced order level where the two equations are considered together.

3. The Reduced Order Model

In this section the derivation of the ROM and the modification one needs to do in order to be able to adapt a standard FEM-Galerkin ROM to a FVM-Galerkin framework is introduced. Here few details are only recalled, for further details one may see [11]. In order to create a ROM that is consistent with the full order model one needs to consider the same methodology used at full order scale. The relevant details introduced here are:

- Introduction of a reduced basis space also for the mass flux term of equation (3) with a similar approach presented also in [11]. This reduced basis space is the one used during the projection phase of the momentum equation.
- Projection of the Poisson equation for pressure reported in Equation (6) onto the POD pressure modes in order to enforce the continuity equation constraint. This approach, that is proposed in literature by several authors [10,18] for FEM approximation, is here adapted to a FVM framework.

The reduced order model is obtained performing a Galerkin projection onto the space spanned by the reduced basis modes and approximating the fields with the following expansions:

$$(7) \quad \begin{pmatrix} \mathbf{u}(\mathbf{x}, t) \\ F(\mathbf{x}, t) \end{pmatrix} \approx \begin{pmatrix} \mathbf{u}_r(\mathbf{x}, t) \\ F_r(\mathbf{x}, t) \end{pmatrix} = \sum_{i=1}^{N_u} a_i(t) \begin{pmatrix} \boldsymbol{\varphi}_i(\mathbf{x}) \\ \psi_i(\mathbf{x}) \end{pmatrix},$$

$$(8) \quad p(\mathbf{x}, t) \approx p_r(\mathbf{x}, t) = \sum_{i=1}^{N_p} b_i(t) \chi_i(\mathbf{x}),$$

where the a_i and b_i are temporal coefficients and $\boldsymbol{\varphi}_i$, ψ_i and χ_i are the modes of the reduced basis spaces for velocity, mass flux and pressure, respectively, N_u and N_p define the dimension of the reduced basis spaces for velocity/mass flux and pressure, respectively. In the above expansions the following assumptions are considered:

- Velocity \mathbf{u} and mass flux F fields are approximated using the same temporal coefficients. This assumption is reasonable since also the mass fluxes over the surfaces of the finite volumes depend strongly on the velocity itself. Moreover the reduced basis space of mass flux and velocity respectively have the same dimension N_u .
- Pressure field p is approximated using different temporal coefficients and for this reason during the projection phase both the momentum conservation and continuity equation must be considered. This

space can have also a different dimension respect to the reduced basis space considered for velocity.

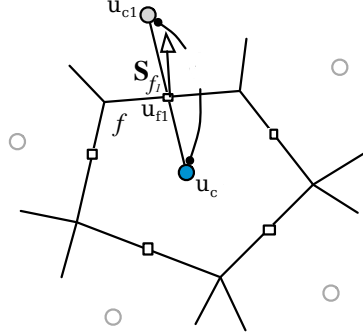


Figure 1. Sketch of a finite volume - Image readapted from [13]

3.1. Generation of the POD spaces

In order to create a reduced basis space onto which the governing equations are projected, one can find many techniques in literature such as the Proper Orthogonal Decomposition (POD), The Proper Generalized Decomposition (PGD), as well as Reduced Basis (RB) method with a greedy approach. For more details about the different methods the reader may see [7,8,19–21]. In this work the POD approach is used. The POD consists into the decomposition of the flow fields into temporal coefficients $a_i(t)$ and orthonormal spatial bases $\varphi_i(\mathbf{x})$:

$$(9) \quad \mathbf{u}(\mathbf{x}, t) = \sum_{i=1}^{N_s} a_i(t) \varphi_i(\mathbf{x}),$$

where $\varphi_i(\mathbf{x})$ are orthonormal spatial bases that minimizes the average of the error between the snapshots and their orthogonal projection onto the bases and N_s is the number of considered snapshots. The POD space $\mathbb{V}_{POD} = \text{span}(\varphi_1, \varphi_2, \dots, \varphi_{N_s})$ is then constructed solving the following minimization problem:

$$(10) \quad \mathbb{V}_{POD} = \arg \min \frac{1}{N_s} \sum_{n=1}^{N_s} \left\| \mathbf{u}_n(\mathbf{x}) - \sum_{i=1}^{N_s} (\mathbf{u}_n(\mathbf{x}), \varphi_i(\mathbf{x}))_{L^2(\Omega)} \varphi_i(\mathbf{x}) \right\|_{L^2(\Omega)}^2,$$

where u_n is a general snapshot of the velocity field at time $t = t_n$. It can be shown that this problem can be solved computing a singular value decomposition $\mathbf{U} = \mathbf{W} \mathbf{\Sigma} \mathbf{V}^T$ of the so called snapshots matrix $\mathbf{U} \in \mathbb{R}^{N_h \times N_s}$.

Where $\mathcal{U} = [\mathbf{u}_1, \mathbf{u}_2, \dots, \mathbf{u}_{N_s}]$ contains the flow fields for all the different time steps, $\mathcal{W}^u \in \mathbb{R}^{N_h \times N_h}$ is a rectangular matrix of left singular vectors, $\mathcal{V}^u \in \mathbb{R}^{N_s \times N_s}$ is a square matrix of right singular vectors, and $\Sigma^u \in \mathbb{R}^{N_h \times N_h}$ is a diagonal matrix of eigenvalues. The POD modes φ_i are then given by the columns of the matrix \mathcal{W}^u . This approach is however computationally very expensive, especially increasing the dimension of the grid used to discretise the domain. An equivalent and more efficient way to tackle this problem, based on the method of snapshots, firstly introduced in [22], consists in solving the eigenvalue problem:

$$(11) \quad \mathbf{C}^u \mathbf{Q}^u = \mathbf{Q}^u \boldsymbol{\lambda}^u,$$

where $\mathbf{C}^u \in \mathbb{R}^{N_s \times N_s}$ is the correlation matrix of the velocity field snapshots, $\mathbf{Q}^u \in \mathbb{R}^{N_s \times N_s}$ is a square matrix whose columns are the eigenvectors and $\boldsymbol{\lambda}^u \in \mathbb{R}^{N_s \times N_s}$ is a diagonal matrix containing the eigenvalues λ_{ii}^u . The correlation matrix can be determined using:

$$(12) \quad C_{ij}^u = (\mathbf{u}_i, \mathbf{u}_j)_{L^2(\Omega)}$$

where $(\cdot, \cdot)_{L^2(\Omega)}$ is the L^2 inner product over the domain Ω . The POD modes can be finally obtained with:

$$(13) \quad \varphi_i = \frac{1}{\sqrt{\lambda_{ii}^u}} \mathcal{U} \mathbf{Q}_i^u.$$

The same procedure can be repeated also for the pressure field considering the matrix $\mathcal{P} = [p_1, p_2, \dots, p_{N_s}]$ one can compute the correlation matrix of the pressure field snapshots \mathbf{C}^p and solve a similar eigenvalue problem $\mathbf{C}^p \mathbf{Q}^p = \mathbf{Q}^p \boldsymbol{\lambda}^p$. The POD modes χ_i for the pressure field can be computed with:

$$(14) \quad \chi_i = \frac{1}{\sqrt{\lambda_{ii}^p}} \mathcal{P} \mathbf{Q}_i^p.$$

The modes for mass flux field are obtained using the same eigenvectors and eigenvalues computed solving the eigenvalue problem of the velocity field and are expressed by:

$$(15) \quad \psi_i = \frac{1}{\sqrt{\lambda_{ii}^u}} \mathcal{F} \mathbf{Q}_i^u,$$

where, again, $\mathcal{F} = [F_1, F_2, \dots, F_{N_s}]$ is a snapshots matrix containing the mass flux field at different time steps.

3.2. Galerkin projection onto the POD space

In this section the Galerkin projection of the governing equations onto the POD space is highlighted and discussed. The idea here is to consider both the momentum conservation and continuity equation. In order to be consistent with the full order solver, the same set of equations are considered, namely the momentum conservation and the Poisson equation for pressure.

3.2.1. Momentum equation

The reduced order model of the momentum equation is obtained performing an L^2 orthogonal projection onto the reduced bases space \mathbb{V}_{POD} spanned by the POD velocity modes with a procedure similar to what presented in [10].

$$(16) \quad (\boldsymbol{\varphi}_i, \mathbf{u}_t + (\mathbf{u} \cdot \nabla)\mathbf{u} - \nu \Delta \mathbf{u} + \nabla p)_{L^2(\Omega)} = 0.$$

Respect to what presented in [10] here also the gradient of pressure is considered inside the momentum equation. This term is considered also in [11] but, there, it is assumed that velocity and pressure modes share the same temporal coefficients. More details about the treatment of this term are given in § 3.2.2. Substituting the POD approximations of \mathbf{u} , F and p into equation (16) and exploiting the orthogonality of the POD modes $\boldsymbol{\varphi}_i$ one obtains the following dynamical system of Ordinary Differential Equations (ODEs):

$$(17) \quad \dot{\mathbf{a}} = \nu \mathbf{B} \mathbf{a} - \mathbf{a}^T \mathbf{C} \mathbf{a} - \mathbf{K} \mathbf{b},$$

where \mathbf{a} and \mathbf{b} are vectors containing all the temporal coefficients $a_i(t)$ and $b_i(t)$ and the terms inside equation (17) read:

$$(18) \quad B_{ij} = (\boldsymbol{\varphi}_i, \Delta \boldsymbol{\varphi}_j)_{L^2(\Omega)},$$

$$(19) \quad C_{ijk} = (\boldsymbol{\varphi}_i, \nabla \cdot (\psi_j, \boldsymbol{\varphi}_k))_{L^2(\Omega)},$$

$$(20) \quad K_{ij} = (\boldsymbol{\varphi}_i, \nabla p_j)_{L^2(\Omega)}.$$

In Equation (19) the term $\nabla \cdot (F, u)$, with an abuse of notation, is used to indicate the convective term, that as indicated in Equation (3) is evaluated using the velocity \mathbf{u} and the mass flux term F .

3.2.2. Poisson equation for pressure

Equation (17) contains N_u equations, given by the momentum equation projected on each of the velocity modes, and $N_u + N_p$ unknowns given by the

temporal coefficients of velocity and pressure. For this reason to close the problem one needs additional equations given by the continuity equation or by the Poisson equation for pressure projected onto the POD pressure space. The additional unknowns inside (17) are given by the gradient of pressure that in many cases is neglected; in fact, in many contributions available in literature no attempt to recover the pressure term is performed. The projection of the pressure gradient onto the POD spaces is in fact zero for the case of enclosed flows as presented in [9,23,24] or in the case of inlet-outlet problems with outlet far from the obstacle [10]. However in many applications the pressure term is needed as highlighted in [25] and cannot be neglected. In the analysed case moreover, since the interest is into the reconstruction of the fluid forces acting onto the cylinder surface, the reconstruction of the pressure term is crucial. According to [18] in literature one can find basically two different approaches for pressure ROMs depending if they use pressure POD modes or not. Among the approaches using pressure modes some work directly on the coupled system composed by the continuity and momentum equation, with the aid of ad hoc stabilization techniques to enforce the well posedness of the problem [18,26,27], and some work with the Poisson equation for pressure [10,18]. On the contrary to what proposed in [11], where only the momentum equation is considered and the assumption that velocity and pressure share the same temporal coefficients is done, here two coefficients depending on time are considered and then the Poisson equation for pressure is exploited. This is projected onto the POD space spanned by the pressure modes χ_i . After integration by part of the Laplacian inside equation (6) term one obtains:

$$(21) \quad (\nabla \chi_i, \nabla p)_{L^2(\Omega)} = (\chi_i, \nabla \cdot ((\mathbf{u} \cdot \nabla) \mathbf{u}))_{L^2(\Omega)},$$

which can be rewritten in matrix form as:

$$(22) \quad \mathbf{D} \mathbf{b} = -\mathbf{E} + \mathbf{a}^T \mathbf{G} \mathbf{a},$$

and the terms inside (22) read:

$$(23) \quad D_{ij} = (\nabla \chi_i, \nabla \chi_j)_{L^2(\Omega)},$$

$$(24) \quad E_i = (\nabla \chi_i, \nabla \bar{p})_{L^2(\Omega)},$$

$$(25) \quad G_{ijk} = (\chi_i, \nabla \cdot (\nabla \cdot (\psi_j, \varphi_k)))_{L^2(\Omega)}.$$

In the above expressions it is done the assumption that the pressure term is decomposed into a mean and a fluctuating term $p = \bar{p} + p'$. The bases for pressure χ_i are then constructed starting from the snapshots matrix of

the fluctuating pressure $\mathcal{P}' = [p'_1, p'_2, \dots, p'_{N_s}]$. The pressure field is then approximated with:

$$(26) \quad p(\mathbf{x}, t) \approx p_r(\mathbf{x}, t) = \bar{p} + \sum_{i=1}^{N_p} b_i(t) \chi_i(\mathbf{x}).$$

3.3. The boundary conditions

In literature different approaches to enforce the BCs in the ROM can be found. In this section it is explained how the Dirichlet boundary conditions are enforced at the reduced order level. The penalty method is used in [11, 28, 29] where the BCs are imposed weakly using a penalty term, however, this method rely on a penalty parameter that has to be tuned with a sensitivity analysis [29]. In this work, in order to enforce the BCs at the ROM level a control function method is used. Within this method, before applying the POD, the inhomogenous boundary conditions are removed from the original snapshots. The problem is then solved and the lifting function is added again to the solution. Only boundary conditions that can be parametrized with a single time-dependent coefficient as in Graham [30] are considered. To retain the divergence-free property of the snapshots the lifting function has also to be divergence free. In particular it is chosen to use as lifting function the arithmetic average of the velocity snapshots, that is opportunely scaled in order to have the desired value at the Dirichlet boundary. Each snapshot of the velocity snapshots matrix is then modified as:

$$(27) \quad \mathbf{u}'_i = \mathbf{u}_i - u_D(t) \phi_c,$$

where ϕ_c is a function that has unitary value at the reference point chosen for the scaling Dirichlet boundary. This lifting function can be evaluated as the arithmetic average of the velocity snapshots \mathbf{u}_m opportunely divided by its own value $u_{m,r}$ at the reference point on the Dirichlet boundary:

$$(28) \quad \phi_c = \frac{1}{N_s u_{m,r}} \sum_{i=1}^{N_s} \mathbf{u}_i.$$

The POD is then applied to the snapshots matrix $\mathcal{U}' = [\mathbf{u}'_1, \mathbf{u}'_2, \dots, \mathbf{u}'_{N_s}]$ that contains only snapshots with homogeneous boundary conditions. The velocity field is then approximated as:

$$(29) \quad \mathbf{u}(\mathbf{x}, t) \approx u_D(t) \phi_c + \sum_{i=1}^{N_u} a_i(t) \varphi_i(\mathbf{x}),$$

Where $u_D(t)$ is a scaling factor depending on time that assumes the value of the Dirichlet BC at the reference point. For sake of simplicity, since time dependent BCs are not considered, the time dependency on $u_D(t)$ will be henceforth omitted. The same procedure is also repeated for the mass fluxes where the term F_c is the mass flux associated with the velocity field ϕ_c and the mass flux is then approximated as:

$$(30) \quad F(\mathbf{x}, t) \approx u_D F_c + \sum_{i=1}^{N_u} a_i(t) \psi_i(\mathbf{x}).$$

During the projection stage illustrated in § 3.2.1 and § 3.2.2 also the above modified approximations of the velocity and mass flux fields have to be considered. The Galerkin projection produces then some additional terms inside the coupled dynamical system that now reads:

$$(31) \quad \begin{cases} \dot{\mathbf{a}} = \mathbf{A}_{BC} + (\mathbf{B} + \mathbf{B}_{BC})\mathbf{a} - \mathbf{a}^T \mathbf{C} \mathbf{a} - \mathbf{K} \mathbf{b} \\ \mathbf{b} = \mathbf{D}^{-1}(\mathbf{E} + \mathbf{E}_{BC} + \mathbf{F}_{BC} \mathbf{a} + \mathbf{a}^T \mathbf{G}_1 \mathbf{a}), \end{cases}$$

where \mathbf{A}_{BC} , \mathbf{B}_{BC} , \mathbf{E}_{BC} and \mathbf{F}_{BC} are equal to

$$(32) \quad \mathbf{A}_{BC} = \nu u_D \mathbf{A}_1 - u_D^2 \mathbf{A}_2,$$

$$(33) \quad \mathbf{B}_{BC} = -u_D \mathbf{B}_1 - u_D \mathbf{B}_2,$$

$$(34) \quad \mathbf{E}_{BC} = u_D^2 \mathbf{E}_1,$$

$$(35) \quad \mathbf{F}_{BC} = u_D(\mathbf{F}_1 + \mathbf{F}_2).$$

The terms are obtained through Galerkin projection of the momentum equation and the Poisson equation for pressure onto the POD velocity and pressure space, respectively:

$$(36) \quad A_{1i} = (\varphi_i, \Delta \phi_c)_{L^2(\Omega)},$$

$$(37) \quad A_{2i} = (\varphi_i, \nabla \cdot (F_c, \phi_c))_{L^2(\Omega)},$$

$$(38) \quad B_{1ij} = (\varphi_i, \nabla \cdot (\psi_j, \phi_c))_{L^2(\Omega)},$$

$$(39) \quad B_{2ij} = (\varphi_i, \nabla \cdot (F_c, \varphi_j))_{L^2(\Omega)},$$

$$(40) \quad E_{1i} = (\chi_i, \nabla \cdot (\nabla \cdot (F_c, \phi_c)))_{L^2(\Omega)},$$

$$(41) \quad F_{1ij} = (\chi_i, \nabla \cdot (\nabla \cdot (\psi_j, \phi_c)))_{L^2(\Omega)},$$

$$(42) \quad F_{2ij} = (\chi_i, \nabla \cdot (\nabla \cdot (F_c, \varphi_j)))_{L^2(\Omega)}.$$

4. A numerical example

In the present section we will discuss the results obtained in the first application of the proposed model reduction procedure for Navier–Stokes

flows. Given all the aforementioned features, the fluid dynamic problem considered is that of the vortex shedding caused by the low Re flow past a circular cylinder with main axis perpendicular to the undisturbed stream velocity \mathbf{U}_∞ . This is a well known and studied benchmark widely discussed and treated in literature from both the experimental and numerical point of view [1]. Due to the considerably larger extension of the cylinder in its axial direction and to the synchronisation observed in the vortices detaching from the cylinder at different axial locations, the vortex shedding mechanism exhibits an intrinsic two-dimensional nature. For such reason, the laminar Navier–Stokes equations (Equation (1)) written in a 2D domain represent a suitable model for the flow at hand. The resulting 2D computational grid is depicted in Figure 2, which also shows the domain height and width as a function of the cylinder diameter $D = 0.027$ m. The structured grid accounts for 13296 quadrilateral cells. The fluid considered in the simulations is water, having constant density $\rho_w = 1000\text{kg/m}^3$ and kinematic viscosity $\nu = 10^{-6}\text{m}^2/\text{s}$. The boundary conditions are set according to Table 1. In each flow simulation, the fluid is started from rest and impulsively accelerated through the imposition of uniform and constant horizontal velocity \mathbf{U}_∞ at the inlet boundary. Each simulation evolves in time until a final periodic regime solution is reached, and is then finally carried on for about 20 to 25 periods. The fluid dynamic drag and lift forces coefficients time history over the latter part of the simulation is then used to carry out Fourier analysis and assess the main vortex shedding frequency.

Table 1. Boundary Conditions

	inlet	outlet	cylinder	sides
\mathbf{u}	$\mathbf{u}_{in} = [u_{x_{in}}, 0]$	$\nabla \mathbf{u} \cdot \mathbf{n} = \mathbf{0}$	$\mathbf{u} = \mathbf{0}$	$\mathbf{u} \cdot \mathbf{n} = 0$
p	$\nabla p \cdot \mathbf{n} = 0$	$p = 0$	$\nabla p \cdot \mathbf{n} = 0$	$\nabla p \cdot \mathbf{n} = 0$

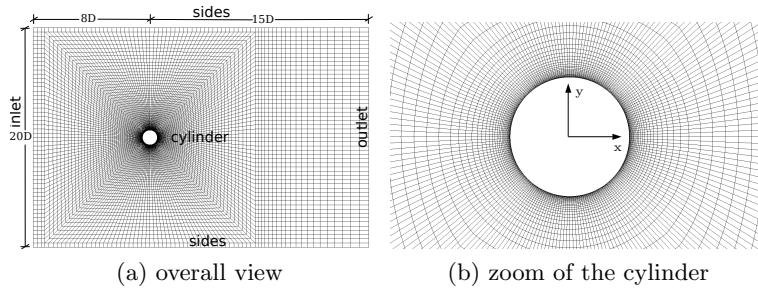


Figure 2. A sketch of the structured computational grid used for the high fidelity simulations. The picture also shows the main dimensions of the computational domain Ω_f , as a function of the cylinder diameter $D = 0.027$ m.

4.1. Constant Inflow Velocity

In this first test case considered, an inlet velocity of $\mathbf{u}_{in} = [3.7\text{e-}3, 0]\text{m/s}$, corresponding to $Re = 100$, is prescribed. The results of the HF simulations at several time instants are then used as the snapshots needed to compute the basis functions and set up the ROM model. Not only the comparison between HF and ROM solution provides a first assessment of the overall ROM performance, but it also helps understanding what is the effect of each ROM parameter on the reduced solution. In particular, we will investigate on the number of bases required for a suitably accurate ROM solution.

4.1.1. Details of the full order simulation

The computational grid is the one presented in § 4. The convective term is discretised in space making use of the Gauss's theorem (see Equation (3)). The face center values of the variables are obtained from the center cell ones, which are the numerical problem unknowns, with an interpolation scheme consisting into a combination of a linear and upwind scheme. The diffusive term is discretised (see Equation (4)) in a similar fashion. In this case though, a central differencing interpolation scheme with non-orthogonality correction is preferred. Also the pressure gradient is discretized making use of Gauss's theorem (see equation (5)). Here, the face center pressure values are obtained from the cell center ones by means of a linear interpolation scheme, in which a limiting operation on the gradient is performed so as to preserve the monotonicity condition and ensure that the extrapolated face value is bounded by the neighbouring cell values. As for the time discretisation, a backward Euler scheme is used. The overall time extent of the simulation is equal to $T = 3645\text{s}$, which is sufficiently long to reach a perfectly periodic response of the lift and drag forces. The simulation is run in parallel on 4 Intel® Core™ i7-4710HQ 2.50GHz processors, taking $T_{CPU_{HF}} = 1483\text{s} \approx 25\text{min}$ to be completed.

4.1.2. Details of the ROM simulation

The ROM is constructed using the methodologies described in § 3. For the generation of the POD spaces, we considered 120 snapshots of the velocity, mass flux and pressure fields. The snapshots are collected in a time window covering approximately 1.5 periods of the vortex shedding phenomenon. More precisely, the last 73s of the HF simulation are used. The first two modes for velocity and pressure field respectively are presented in Figure 3 and 4. The ROM simulations are carried out using different values of the POD velocity space dimension $N_u = 3, 5, 7, 10$. The dimension of the

POD pressure and mass flux space is set equal to the dimension of the velocity POD space $N_u = N_p$. The ROM simulation is run in serial, on the same processor used for the HF simulation. In this case, the time advancing of the ROM problem is carried out using the Matlab ODE suite [31]. Reproducing the full 3645s extent of the high fidelity simulation requires, using the ROM model with the highest dimension of the POD space, approximately $T_{CPU_{ROM}} = 9.10s$. This corresponds to a speedup $SU \approx 650$.

4.1.3. Analysis of the results

Using the settings described in the previous paragraph, four different ROM simulations are run, each featuring a different value of the POD space dimension. The results are compared with those of the HF simulation in terms of history of the lift and drag coefficients. The time window used for the comparison is the same window used for the collection of the snapshots. The lift coefficient comparison is reported in Figure 5, while the drag coefficient time histories is presented in Figure 6. In each Figure, the four different plots refer to the four different values of the POD space dimensions considered in the ROM simulations. Finally, in Figure 7 the comparison is shown directly on the velocity and the pressure fields. In this case, the time step considered is the last one of the simulations, corresponding to $T = 3645s$. The left plot in Figure 7 refer to the velocity (top) and pressure (bottom) fields computed with the high fidelity simulations. The right plots refer to the velocity (top) and pressure (bottom) fields computed with the ROM, in which the POD space dimension has been set to $N_u = 10$. The plots show that, at a glance the HF and ROM solutions cannot be distinguished.

To provide a more quantitative evaluation of the error in the force coefficients reconstruction, for each ROM simulation we computed the Weighted Absolute Percentage Error (WAPE) with respect to the HF simulations. For the case of the lift coefficient the WAPE has been directly applied to the lift signal without any modification, namely

$$(43) \quad \varepsilon_{L_c} = \frac{100}{n} \sum_{t=1}^n \left| \frac{L_{c_t}^{HF} - L_{c_t}^{ROM}}{\overline{L_c^{HF}}} \right| \%$$

where n_t is the number of sampling points, $L_{c_i}^{HF}$ and $L_{c_i}^{ROM}$ are the lift coefficients for the HF and ROM case respectively at the i -th time step. For the case of the drag coefficient, the WAPE has been applied to D'_c that is the value of the drag shifted by its mean value $D'_c = D_c - \overline{D_c}$. From table 2 and Figures 5–6 one can see that, for the present case, adding more than 7 modes does not increase the accuracy of the ROM results.

Vortex shedding around a circular cylinder using a POD-Galerkin method

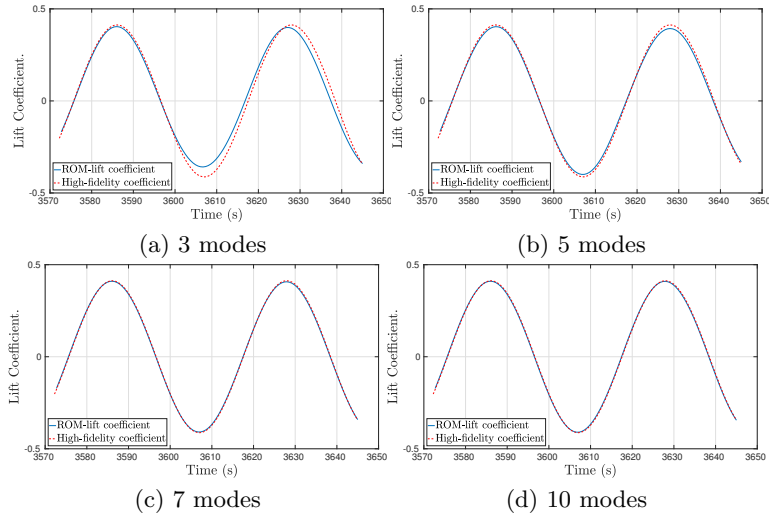
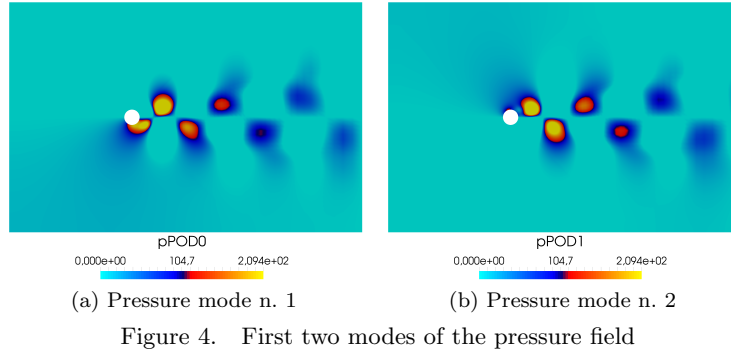
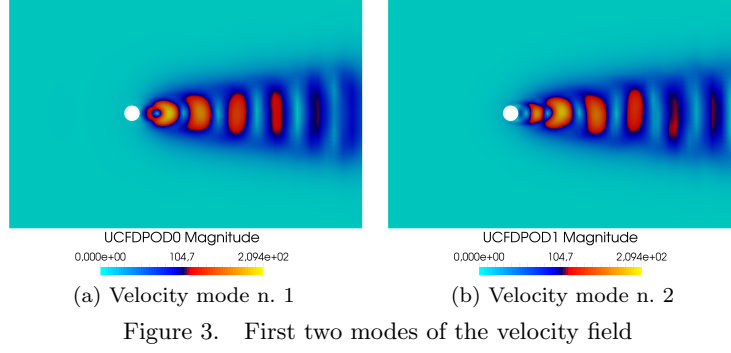


Table 2. Error on L_c and D_c using different dimensions of the POD spaces

	$N_u = N_p = 3$	$N_u = N_p = 5$	$N_u = N_p = 7$	$N_u = N_p = 10$
$\varepsilon_{L_c}(\%)$	11.50	4.32	1.59	1.89
$\varepsilon_{D_c}(\%)$	64.49	13.94	4.69	6.43

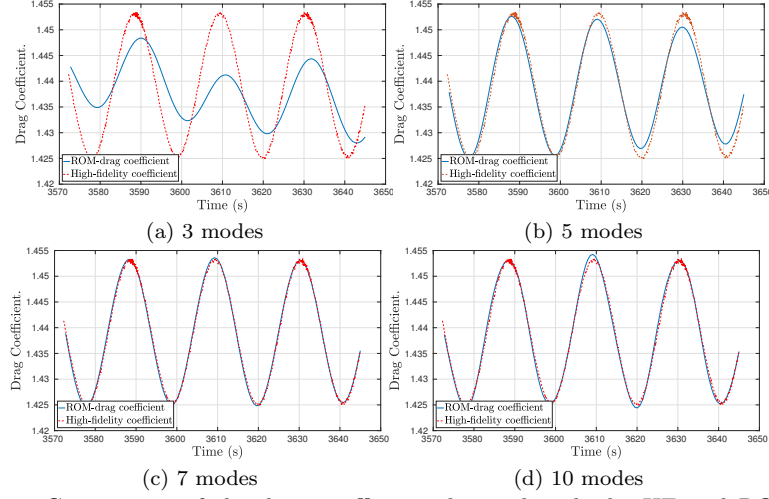


Figure 6. Comparison of the drag coefficient obtained with the HF and ROM simulations. The comparison is plotted on the same window used for the collection of the snapshots

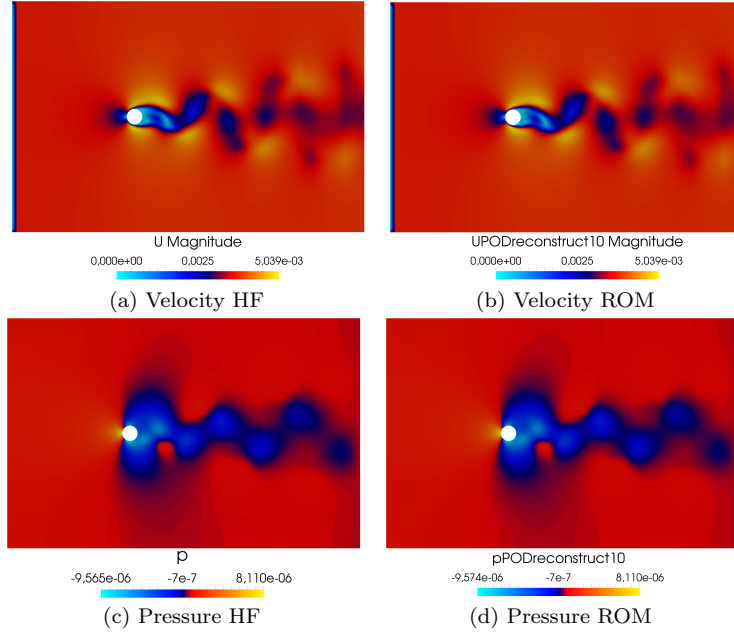


Figure 7. Comparison between velocity and pressure HF-ROM

4.2. Varying Inflow Velocity

In the second example the inlet velocity is used as a physical parameter and the HF simulations are performed using five different values of the

Vortex shedding around a circular cylinder using a POD-Galerkin method

Reynolds number $Re = [100, 125, 150, 175, 200]$. Using the same procedure described in § 4.1, 120 snapshots are collected for each different value of Re . Thus, the POD is performed on the resulting ensemble of 600 snapshots gathered from the 5 different HF simulations. According to the results presented in § 4.1, 7 modes for each different velocity are considered. In this case, leading to a total number of modes equal to 35. The computational details of the HF simulations are the same described in § 4.1. Once the offline phase is carried out and the ROM is set up, several reduced simulations are performed. Such simulations are also featuring inlet velocities that correspond to *Reynolds* numbers which were not considered in the HF analysis. Thus, this numerical experiment is devised to test if the ROM developed is able to reproduce the dependence of the system output with respect to an input parameter such as the velocity of the stream in which the cylinder is embedded. The comparison between the HF and ROM simulations is performed comparing the frequency corresponding to the peak of the power spectral density of the lift coefficient. Investigating such dependence is particularly important, as variations in the main stream velocity might result in different frequency components in the hydrodynamic force on the cylinder. By an engineering standpoint, it is typically very important to assess whether such frequency components are close to the structural natural frequency and might lead to resonance. The comparison can be seen in Figure 8 where the blue line with circles and the red line with stars refer respectively to the results of ROM and HF simulations. As one observes from the figure the ROM simulations match well the HF simulations that for this range of *Reynolds* numbers lay on the red straight line.

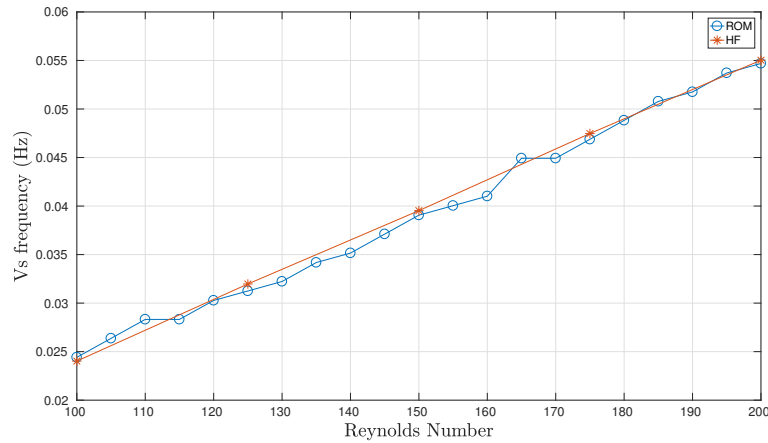


Figure 8. Comparison of ROM and HF for the case of increasing velocities - frequency of vortex shedding

5. Conclusions and future developments

In this work a POD-Galerkin ROM based on finite volume high fidelity simulations is presented. The ROM is generated such that to be fully consistent with the full order model, and both velocity and pressure fields are considered. In particular, the reconstruction of the reduced pressure field is carried out through the projection of the Poisson equation for pressure onto the POD pressure space. The ROM is then applied to approximate the unsteady viscous flow around a circular cylinder. In particular, the focus and originality is into the accurate reproduction of the lift and drag forces associated with the vortex shedding phenomenon. The ROM developed demonstrated to be capable of reproducing all the main features of the physical phenomenon in an accurate manner leading to a considerable computational time reduction (speedup $SU \approx 650$). Also in the case of varying inflow velocities the ROM has demonstrated the ability of capturing the dependence of frequency of vortex shedding on the inflow velocity. As future developments the interest is into different efficient methodologies for the reconstruction of the pressure term and in particular to study the applicability of well known stabilization methods, used by the FEM-ROM community [26,27], to a FV-Galerkin framework [32]. The interest is also in the study of the same physical problem, but where the fluid-structure interaction problem is also considered. This will introduce additional complexities such as the mesh motion and additional equations to account for the structural dynamics and the fluid structure interaction coupling. Adding also the structural part to the ROM will be essential to tackle real-world engineering problems.

Acknowledgements

We acknowledge the support provided by the European Research Council project Advanced Reduced Order Methods with Applications in Computational Fluid Dynamics - GA 681447, H2020-ERC COG 2015 AROMA-CFD and INdAM-GNCS.

6. Bibliography.

REFERENCES

1. M. P. Païdoussis, *Fluid-Structure Interactions. Slender Structures and Axial Flow. Volume 1*. Academic Press, first ed., 1998.
2. M. P. Païdoussis, *Fluid-Structure Interactions. Slender Structures and Axial Flow. Volume 2*. Academic Press, first ed., 2003.

3. V. Strouhal, Über eine besondere Art der Tonerregung, *Annalen der Physik*, vol. 241, no. 10, pp. 216–251, 1878.
4. R. T. Hartlen and I. G. Currie, Lift-oscillator model of vortex-induced vibration, *Journal of the Engineering Mechanics Division*, vol. 96, no. 5, pp. 577–591, 1970.
5. M. Facchinetti, E. de Langre, and F. Biolley, Coupling of structure and wake oscillators in vortex-induced vibrations, *Journal of Fluids and Structures*, vol. 19, no. 2, pp. 123 – 140, 2004.
6. G. Stabile, H. G. Matthies, and C. Borri, A novel reduced order model for vortex induced vibrations of long flexible cylinders, *Submitted to Journal of Ocean Engineering*, 2016.
7. J. S. Hesthaven, G. Rozza, and B. Stamm, *Certified Reduced Basis Methods for Parametrized Partial Differential Equations*. Springer International Publishing, 2016.
8. A. Quarteroni, A. Manzoni, and F. Negri, *Reduced Basis Methods for Partial Differential Equations*. Springer International Publishing, 2016.
9. B. R. Noack and H. Eckelmann, A low-dimensional Galerkin method for the three-dimensional flow around a circular cylinder, *Physics of Fluids*, vol. 6, no. 1, pp. 124–143, 1994.
10. I. Akhtar, A. H. Nayfeh, and C. J. Ribbens, On the stability and extension of reduced-order Galerkin models in incompressible flows, *Theoretical and Computational Fluid Dynamics*, vol. 23, no. 3, pp. 213–237, 2009.
11. S. Lorenzi, A. Cammi, L. Luzzi, and G. Rozza, POD-Galerkin method for finite volume approximation of Navier-Stokes and RANS equations, *Computer Methods in Applied Mechanics and Engineering*, vol. 311, pp. 151 – 179, 2016.
12. H. K. Versteeg and W. Malalasekera, *An Introduction to Computational Fluid Dynamics. The Finite Volume Method*. London: Longman Group Ltd., 1995.
13. F. Moukalled, L. Mangani, and M. Darwish, *The Finite Volume Method in Computational Fluid Dynamics: An Advanced Introduction with OpenFOAM and Matlab*. Springer Publishing Company, Incorporated, 1st ed., 2015.
14. H. G. Weller, G. Tabor, H. Jasak, and C. Fureby, A tensorial approach to computational continuum mechanics using object-oriented techniques, *Computers in physics*, vol. 12, no. 6, pp. 620–631, 1998.
15. “OpenFOAM documentation website.” <http://www.openfoam.com/documentation/>. Accessed: 20-12-2016.
16. R. I. Issa, Solution of the Implicitly Discretised Fluid Flow Equations by Operator-splitting, *J. Comput. Phys.*, vol. 62, pp. 40–65, Jan. 1986.

17. S. Patankar and D. Spalding, A calculation procedure for heat, mass and momentum transfer in three-dimensional parabolic flows, *International Journal of Heat and Mass Transfer*, vol. 15, no. 10, pp. 1787 – 1806, 1972.
18. A. Caiazzo, T. Iliescu, V. John, and S. Schyschlowa, A numerical investigation of velocity-pressure reduced order models for incompressible flows, *Journal of Computational Physics*, vol. 259, pp. 598 – 616, 2014.
19. G. Rozza, D. Huynh, and A. Patera, Reduced basis approximation and a posteriori error estimation for affinely parametrized elliptic coercive partial differential equations: Application to transport and continuum mechanics, *Archives of Computational Methods in Engineering*, vol. 15, no. 3, pp. 229–275, 2008. cited By 292.
20. F. Chinesta, A. Huerta, G. Rozza, and K. Willcox, Model Order Reduction, *Encyclopedia of Computational Mechanics*, In Press, 2017.
21. F. Chinesta, P. Ladeveze, and E. Cueto, A Short Review on Model Order Reduction Based on Proper Generalized Decomposition, *Archives of Computational Methods in Engineering*, vol. 18, no. 4, p. 395, 2011.
22. L. Sirovich, Turbulence and the Dynamics of Coherent Structures part I: Coherent Structures, *Quarterly of Applied Mathematics*, vol. 45, no. 3, pp. 561–571, 1987.
23. A. E. Deane, I. G. Kevrekidis, G. E. Karniadakis, and S. A. Orszag, Low-dimensional models for complex geometry flows: Application to grooved channels and circular cylinders, *Physics of Fluids A: Fluid Dynamics*, vol. 3, no. 10, pp. 2337–2354, 1991.
24. X. Ma and G. Karniadakis, A low-dimensional model for simulating three-dimensional cylinder flow, *Journal of Fluid Mechanics*, vol. 458, pp. 181–190, 2002. cited By 170.
25. B. R. Noack, P. Papas, and P. A. Monkewitz, The need for a pressure-term representation in empirical Galerkin models of incompressible shear flows, *Journal of Fluid Mechanics*, vol. 523, pp. 339–365, 01 2005.
26. F. Ballarin, A. Manzoni, A. Quarteroni, and G. Rozza, Supremizer stabilization of POD-Galerkin approximation of parametrized steady incompressible Navier–Stokes equations, *International Journal for Numerical Methods in Engineering*, vol. 102, no. 5, pp. 1136–1161, 2015.
27. G. Rozza and K. Veroy, On the stability of the reduced basis method for Stokes equations in parametrized domains, *Computer Methods in Applied Mechanics and Engineering*, vol. 196, no. 7, pp. 1244 – 1260, 2007.
28. I. Kalashnikova and M. F. Barone, On the stability and convergence of a Galerkin reduced order model (ROM) of compressible flow with solid wall and far-field boundary treatment, *International Journal for Numerical Methods in Engineering*, vol. 83, no. 10, pp. 1345–1375, 2010.

29. S. Sirisup and G. Karniadakis, Stability and accuracy of periodic flow solutions obtained by a POD-penalty method, *Physica D: Nonlinear Phenomena*, vol. 202, no. 3-4, pp. 218 – 237, 2005.
30. W. R. Graham, J. Peraire, and K. Y. Tang, Optimal control of vortex shedding using low-order models. Part I: open-loop model development, *International Journal for Numerical Methods in Engineering*, vol. 44, no. 7, pp. 945–972, 1999.
31. L. F. Shampine and M. W. Reichelt, The MATLAB ODE Suite, *SIAM Journal on Scientific Computing*, vol. 18, no. 1, pp. 1–22, 1997.
32. G. Stabile and G. Rozza, Stabilized Reduced order POD-Galerkin techniques for finite volume approximation of the parametrized Navier–Stokes equations, *in preparation*, 2017.